A multi-temporal method for cloud detection, applied to FORMOSAT-2, VENµS, LANDSAT and SENTINEL-2 images

Olivier Hagolle, Mireille Huc, Villa Pascual David, Gérard Dedieu

▶ To cite this version:

HAL Id: hal-00489793

https://hal.archives-ouvertes.fr/hal-00489793

Submitted on 29 Nov 2012

1   # A multi-temporal method for cloud detection, applied to FORMOSAT-2,

2   # VENµS, LANDSAT and SENTINEL-2 images

3

4   O. Hagolle[1,2], M. Huc[2] , D.Villa Pascual[1], G. Dedieu[2]

5   1 CNES, 18 avenue Edouard Belin, 31401 TOULOUSE Cedex 4. Olivier.Hagolle@cnes.fr

6   2 CESBIO, Université de Toulouse, Unité mixte CNES CNRS IRD UPS, 18, avenue Edouard Belin, 31401

7   Toulouse Cedex 4, France

8

9   ABSTRACT –

10   *Over lands, the cloud detection on remote sensing images is not an easy task, because of the*

11   *frequent difficulty to distinguish clouds from the underlying landscape, even at a high resolution.*

12   *Up to now, most high resolution images have been distributed without an associated cloud mask.*

13   *This situation should change in the near future, thanks to two new satellite missions that will*

14   *provide optical images combining 3 features : high spatial resolution, high revisit frequency and*

15   *constant viewing angles. The VENµS (French and Israeli cooperation) mission should be launched*

16   *in 2012 and the European SENTINEL-2 mission in 2013. Fortunately, two existing satellite*

17   *missions, FORMOSAT-2 and LANDSAT, enable to simulate the future data of these sensors.*

18   *Multi-temporal imagery at constant viewing angles provides a new way to discriminate clouded*

19   *and unclouded pixels, using the relative stability of the earth surface reflectances compared to the*

20   *quick variations of the reflectance of pixels affected by clouds. In this study, we have used time*

21   *series of images from FORMOSAT-2 and LANDSAT to develop and test a Multi-Temporal Cloud*

22   *Detection (MTCD) method. This algorithm combines a detection of a sudden increase of reflectance*

23   *in the blue wavelength on a pixel by pixel basis, and a test of the linear correlation of pixel*

24   *neighborhoods taken from couples of images acquired successively.*

25   *MTCD cloud masks are compared with cloud cover assessments obtained from FORMOSAT2 and*

26   *LANDSAT data catalogs. The results show that the MTCD method provides a better discrimination*

27   *of clouded and unclouded pixels than usual methods based on thresholds applied to reflectances or*

28 *reflectance ratios. This method will be used within VENµS level 2 processing and will be proposed*

29 *for SENTINEL-2 level 2 processing.*

1.Introduction

31 Cloud detection is one of the first difficulties encountered when trying to automatically process

32 optical remote sensing data ; for instance, atmospheric correction, land cover classifications, change

33 detection or inversion of biophysical variables require a preliminary step of cloud detection. Cloud

34 detection is easier above water, because water has a uniform and low reflectance in the near infrared

35 (except in sun glint geometry), but is much more difficult over land : even at high resolution, when

36 clouds are much larger than pixel size, it is not easy to tell some thin clouds apart from the

37 underlying landscape.

38 Most of the currently operational cloud screening methods were developed for moderate resolution

39 sensors. The algorithms are highly dependent on the available spectral bands, many of them work

40 on pixel by pixel basis (Bréon and Colzy, 1999, Lissens et al, 2000), some use neighborhood

41 information, such as local standard deviation (Saunders and Kriebel, 1988, Ackerman et al, 1998).

42 When available, thermal infrared bands are used to detect clouds colder than the earth surface,

43 which corresponds to almost all types of clouds except thin or low clouds (Saunders and Kriebel,

44 1988, Ackerman et al 1998). Thresholds on reflectance in the blue are better suited to detect low

45 clouds, but they may fail when the earth surface is bright (Bréon and Colzy, 1999). Short Wave

46 Infra Red (SWIR) bands are often used to tell snow apart from clouds : these targets have similar

47 reflectance ranges in the visible and near infrared, but the SWIR reflectance of snow is much lower

48 than that of clouds (Dozier, 1989). Among the SWIR bands, the 1380 nm band is located in a very

49 strong water vapor absorption band, such that only the upper layers of the atmosphere are visible

50 and the background is completely black. This band has been successfully used for MODIS project

51 to detect high clouds (Gao et al, 1993), and the method works well even with thin cirrus clouds

52 which are very difficult to detect otherwise (Lavanant, 2007).

53 Only a few algorithms use multi temporal observations to detect clouds : some of them compare the

54   processed product to a multi year monthly average of surface reflectance (Ackerman et al, 1998,

55   Bréon and Colzy, 1999) ; Lyapustin et al 2008 relied on the hypothesis that the presence of a cloud

56   is likely if a low correlation is observed at local scale between two successive images of the same

57   zone; Reuter and Fisher, 2004, used the smooth variations of land surface temperatures observed

58   within a day, to classify outliers as clouds on Meteosat Geostationary satellite images.

59   Until recently, given the cost of high resolution images, most users only ordered images with a very

60   low cloud cover, and moreover, very few users have had access to time series with more than 10

61   images. For such a small number of images, it is possible to discard the clouds manually (see for

62   instance Wilson and Sader, 2002). Consequently, very few studies focused on the automatic cloud

63   detection at high resolution (Wang et Ono, 1999). Space agencies and image distributors have

64   developed algorithms to deliver a cloud notation within their image catalogs (Irish, 2000, Irish et al,

65   2006, Latry et al, 2007), but their aim is only to help the user to choose the images to order : no

66   cloud mask is provided with LANDSAT and SPOT products.

67   In 2009, the LANDSAT archive images became freely available, and in the near future, time series

68   of VENµS (Dedieu et al 2006) and SENTINEL-2 (Martimor et al 2007) images will also be freely

69   delivered to research users at least. As a result, time series of 50 to 100 images will become

70   common, and an automatic cloud detection will be requested both by users and for the production of

71   higher level products.

72   One important and original characteristic of VENµS and SENTINEL-2 images is that a given site

73   will be acquired with constant observation angles at a constant local hour, and thus the directional

74   effects (Roujean et al, 1992, Maignan et al, 2004) will be minimized. And thanks to the use of a

75   sun-synchronous orbit, the variation of sun angles is also quite slow (near the equinoxes at 45°

76   latitude, it can reach 10 degrees in a month). The surface reflectance variations above land due to

77   sun angle variations within a month are usually below 5%, except near the backscattering direction

78   (5 to 10 degrees distance). Backscattering observations are not possible for LANDSAT, they were

79   avoided for our FORMOSAT time series and they will be avoided with VENµS. The surface

80   reflectance of a land pixel usually varies very slowly with time, especially at short wavelengths

81   (400-500nm). As a result, a significant increase of reflectance in this wavelength range is very

82   likely to be due to the appearance of a cloud. This criterion should provide a better discrimination

83   than the classical approaches based on a threshold on reflectance in the blue spectral bands.

84   The Multi Temporal Cloud Detection (MTCD) method presented hereafter will be included in

85   VENµS operational level 2 processing, as a preliminary step of the atmospheric correction. The

86   atmospheric correction also is based on a multi-temporal method (Hagolle et al, 2008) and requires

87   a very strict cloud mask. The MTCD mask will also be used to compute level 3 products (cloud free

88   time composites) and it will be distributed to the users with each level 2 product. A cloud shadow

89   detection has also been developed, based on the geometrical projection of the clouds detected,

90   similarly to the work of Le Hegarat-Mascle, 2009, but describing this algorithm is out of the scope

91   of the paper.

92   The next chapters detail successively the data sets, the cloud detection method, and the results we

93   obtained.

94

2. Data Sets used in the study

Table 1 summarizes the characteristics of the sensors used for this study. VENµS (Dedieu et al, 2006) is a scientific micro-satellite that results from a cooperation between the Israeli Space Agency (ISA) and the French Centre National d'Etudes Spatiales (CNES). VENµS will be launched no sooner than 2012. Its aim is to demonstrate the usefulness of repetitive acquisitions of high resolution images to monitor the dynamics of land surfaces, and especially vegetation. At least fifty sites around the world will be imaged by VENµS, every second day, during two years. The resolution of VENµS products will be 10m, with a field of view of 27km. Thanks to the orbital repeat cycle of 2 days, a given site will be observed with a constant viewing angle. The instrument will deliver images in 12 narrow spectral bands ranging from 415 nm to 910 nm.

The SENTINEL-2 satellites (Martimor et al, 2007) will generalize VENµS measurements to the whole land surfaces : it is an operational mission from the European Space Agency (ESA), based on two satellites scheduled to be launched respectively in 2013 and 2014. SENTINEL-2 will acquire high resolution images (10 to 60 m depending on the spectral band), with a field of view of 300 km. The orbital repeat cycle is 10 days and 2 satellites will be placed on that orbit with a 180° angular distance: the two satellites will achieve a 5 days revisit period. As all the images will be acquired at Nadir, a given point on the earth will be observed at a constant viewing angle. The thirteen spectral bands of SENTINEL-2 range from visible to SWIR and are listed in table 1.

FORMOSAT-2 is a Taiwanese Satellite that provides data very similar to VENµS. It is possible to obtain 8m resolution images, every day, with constant viewing angles since FORMOSAT-2 orbit has a one day repeat cycle. The field of view is 24 km, and 4 spectral bands (490, 560, 660 and 820 nm) are available. Up to now, given the cost of each image, few users have ordered such time series yet.

In the framework of VENµS preparation, CNES has purchased about 10 such time series, with a tentative acquisition every 5 days on average, and observation durations from 2 months to 4 years. These time series correspond to very different sites such as agricultural sites in temperate regions, a

121 conifer forest, agricultural sites in semi arid regions, mountains with snow , and a Sahelian site. For

122 two of these sites (Muret, South west France, and Tensift, Morocco), in 2006, we ordered for a

123 systematic acquisition and production of images, cloudy or not, while for the other sites and the

124 other years, for cost reasons, only images with low cloud coverage were purchased. For this reason,

125 only Muret and Tensift time series are fully suited to validate the cloud cover estimates in cloudy,

126 clear and mixed cases (See table 2 for site coordinates). FORMOSAT-2 images were ordered at

127 level 1A and were orthorectified and registered using the algorithms of Baillarin et al, 2008. The

128 absolute calibration of the sensor was obtained using the desert sites method (Cabot et al, 2000). 30

129 to 50 images are available for both sites.

130 As FORMOSAT-2 lacks SWIR bands, it is not perfectly suited to simulate SENTINEL-2 time series

131 and to test the enhancements brought by these bands. For this purpose, we use time series acquired

132 between 1999 and 2003, combining LANDSAT 5 Thematic Mapper and LANDSAT 7 Enhanced

133 Thematic Mapper data, when both instruments were fully operational (cf LANDSAT Handbook).

134 We have used 3 data sets taken by both LANDSAT satellites during the whole year 2002, in the

135 USA : Fresno, Boulder, Columbia (See table 2 for sites coordinates). These products are

136 orthorectified and calibrated (L1T products). On average, each time series is made of about 35 non

137 completely cloudy images.

3. Multi Temporal Cloud Detection (MTCD) method

139 Compared to MODIS and LANDSAT, VENμS and FORMOSAT-2 lack thermal infra-red and short

140 wave infrared bands. VENμS and FORMOSAT-2 have spectral bands in the blue, but it is well

141 known that the histograms for clouds and surface reflectances overlap to such an extent that thin

142 clouds or bright land surfaces may often be confused (Bréon and Colzy 1999). For instance, figure 1

143 shows the histogram overlap of blue reflectance, for a FORMOSAT-2 scene in Tensift, in a hard

144 case (bright ground, thin clouds). On the same figure (bottom plot), one can note a better histogram

145 separation for the reflectance difference between two successive acquisitions. In this figure, the

146 cloud notation results from our method described below, but the validity of the cloud classification

147 has been checked by visual inspection, as it may be seen on figure 2.

148 As a result, our main criterion to detect clouds is a threshold on the reflectance increase in the blue

149 spectral band. To compute the variations and detect clouds for the image of day D, a cloud free

150 reference image is needed, and as it is not always available, it has to be build from partly cloudy

151 images. Our clear image is a composite image that contains for each pixel the most recent cloud free

152 reflectance obtained in the time series before date D. Our algorithm works at 100m resolution for

153 FORMOSAT2 and 240m for LANDSAT, mainly for computing performance reasons, but also to

154 avoid possible image registration errors. A pixel is flagged as cloudy for the multi temporal criterion

155 if :

156 $$\left[\rho_{\text{blue}}(D) - \rho_{\text{blue}}(D_r)\right] > 0.03 * \left(1 + (D - D_r)/30\right) \text{ (1)}$$

157 where $\rho_{\text{blue}}(D)$ is the pixel reflectance in the blue band, corrected for Rayleigh scattering,

158 at date D, and D_r is the date of the most recent cloud free data before date D; D- D_r is expressed in

159 days. The threshold value depends on the number of days between D and D_r . When dates are very

160 close, the threshold tends to 0.03, but this value doubles when D_r and D are separated by 30 days,

161 to allow a change in surface reflectances.

162 Although this criterion proves very efficient to separate cloudy and cloud free pixels above land

163 surfaces, it is of course not foolproof. First, it does not work well above inland water surfaces,

164 which are prone to sudden variations of reflectance because of sunglint, turbidity or foam. Water

165 pixels must be discarded before computing the cloud mask. Second, thin clouds and high aerosol

166 optical thicknesses may be confused : some clouds may be too thin to be detected (see Fig 4),

167 whereas high variations of AOT may be regarded as clouds. Third, sudden variations of surface

168 reflectances may occur, due to agricultural interventions (cropping, ploughing), or to natural

169 variations such as fires or snow, or just to a quick drying of vegetation. To cope with these

170 problems, two tests were added to check if a sudden reflectance increase is really due to a cloud. A

171 pixel that verifies equation (1) is finally not flagged as cloudy if any of the 2 following conditions is

172 true :

173 •i) If the variation of reflectance in the red band is much greater than the reflectance variation in the

174 blue : this happens quite often when a field is cropped or ploughed, or when vegetation dries

175 quickly.

176 $\rho_{\text{red}}(D) - \rho_{\text{red}}(D_r) > 1.5 * (\rho_{\text{blue}}(D) - \rho_{\text{blue}}(D_r))$ (2)

177   where $\rho_{red}(D)$ is the pixel TOA reflectance in the red band, corrected from

178 Rayleigh scattering.

179 •ii) if the reflectances in the pixel neighborhood are well correlated with those of the same

180 neighborhood in one of the ten images acquired before date D. Such a test was already used by

181 Lyapustin et al, 2008 : as it is very unlikely that a cloud stays at the same place with a constant

182 shape, a good correlation coefficient can only be due to a good transparency of the atmosphere.

183 Using the ten previous images instead of the composite images enables to cope with a possible

184 initial error in the composite. For instance, a case was found in which plastic greenhouses were

185 installed on a field : the condition of equation (1) is met and the pixel is flagged as cloudy. Being

186 cloudy, the pixel is not used to update the composite, and the subsequent days would still be

187 flagged as cloudy because the condition of equation (1) would remain true. Since the correlation

188 between two successive images with the greenhouse is high, the criterion ii) reclassifies the pixel as

189 unclouded. Thanks to that, the greenhouse is only marked as a cloud on a single date, instead of a

190 long duration. This scheme can also work with snow, provided the snow cover does not change

191 much after the fall. This correlation test also enables to classify as unclouded the images with a high

192 AOT, but it sometimes reclassifies as unclouded the images with very thin clouds. Finally, we found

193 out that images with an AOT under 0.7 at 550 nm are classified as unclouded whereas images with

194 an AOT above 1 are classified as mostly cloudy. But this assertion is based on a very limited

195 number of images, because of the scarcity of high AOT images on our time series.

196 The MTCD method is a recurrent algorithm for which the images must be processed in

197 chronological order ; as any recurrent process, our algorithm needs to be initialized. The first cloud

198 mask of the first image in the time series is obtained by a simple threshold on the blue band

199 reflectance, and the first composite image is thus the first image, without the cloudy pixels. In order

200 to be conservative, the threshold is quite high so that bright surface reflectances are not classified as

201 cloudy. As a consequence, thin clouds are missed in this first cloud mask. To avoid a degraded

202 quality for the first images of a time series, we have implemented a "backward processing" scheme.

203 The first 6 to 10 images are processed in reverse chronological order, so that a correct cloud mask is

204 obtained for the first image of the time series. Then, all the images of the time series are processed

205 in chronological order, starting with a cloud mask of good quality.

206 Finally, as LANDSAT and Sentinel-2 sensors include FORMOSAT spectral bands in their band

207 setting, our algorithm is also fully applicable to LANDSAT and Sentinel 2, although with a

208 somewhat reduced accuracy because of the reduced revisit frequency. We did not use LANDSAT

209 TIR (Thermal Infrared) band because our algorithm is intended to be implemented for VENµS and

210 SENTINEL-2, for which no TIR band is available. On the other hand, LANDSAT SWIR bands are

211 used to separate snow and clouds, following the method of Irish, 2000. The snow test is based on

212 the Normalized Difference Snow Index (NDSI), defined as :

213 $: NDSI = \dfrac{\rho_{\text{Green}}(D) - \rho_{\text{SWIR}}(D)}{\rho_{\text{Green}}(D) + \rho_{\text{SWIR}}(D)}$

214 where $\rho_{Green}(D)$ (resp. $\rho_{SWIR}(D)$)is the TOA reflectance in LANDSAT green channel

215 (resp. LANDSAT SWIR channel at 1.6µm). Clouds and snow reflectances are high in the green

216 band, but snow reflectance is much lower in the SWIR. As a result, a bright pixel is flagged as snow

217 if NDSI >0.6.

218 Finally, the cloud masks are dilated since it is very common to observe thin clouds at the edge of

219 thicker clouds. Dilatation is 2-pixel wide at reduced resolution, ie 200m for FORMOSAT-2 and

220 480m for LANDSAT.

4. Algorithm assessment

222 The validation of a cloud mask is a hard task. First, there is a continuity between haze and clouds,

223 and defining a precise limit between them is subjective. Second, there is no reliable independent

224 source of cloud mask at a given hour : all remote sensing cloud masks are imperfect, and ground

225 truths, for instance using a ground based Lidar, only provide a very local information not suitable

226 for a comparison with a high resolution image. Bréon and Colzy (1999) have used synoptic

227 observations from weather stations, but those only provide an average idea of the cloud cover in the

228 vicinity of the station, which cannot be used to validate a high resolution cloud mask.

229 Lavanant et al, 2007 have used a data set of more than ten thousand low resolution vignettes

230 classified by specialized photo interpreters to test their algorithms. Our algorithms have been

231 applied to more than 300 FORMOSAT-2 images and more than 100 LANDSAT Images, and

232 validated visually, but of course, it is not possible to show all these images here. For FORMOSAT-2

233 satellite, Taiwan National Space Organization (NSPO) performs a cloud notation on all the images :

234 an operator simply estimates visually the cloud cover percentage on each image. Figure 4 compares

235 the cloud percentage from MTCD method to that of NSPO, for the Tensift and Muret sites. The

236 agreement is surprisingly good given the rough estimate made by NSPO. Disagreements are only

237 observed in a small number of cases : some of them are shown on fig 4, with the MTCD contour

238 overlaid. On most cases, MTCD cloud notation seems more accurate.

239 We followed the same method to validate the MTCD masks obtained with LANDSAT. The

240 independent notation is issued from the Automatic Cloud Cover Assessment (ACCA, Irish et al,

241 2006), and thus is not a result of photo interpretation. The ACCA algorithm makes an intensive use

242 of LANDSAT thermal infrared band. The method applied to LANDSAT 7 is a refined version

243 compared to LANDSAT 5 ; an assessment of those algorithms is available in Hollingsworth et al,

244 1996. The authors show that compared to photo interpretation, these algorithms slightly

245 underestimate the cloud cover, which is consistent with the results obtained on figures 6, 7, 8 and 9.

246 Figure 6 shows a good agreement for the simple cases with very low or very high cloud covers, but

247 the MTCD cloud cover is often greater than the cloud cover estimate from LANDSAT. Compared to

248 MTCD, the ACCA algorithm seems to underestimate the cloud cover. Although there are some

249 outliers, the agreement is generally better with LANDSAT 7 than with LANDSAT 5, which is

250 consistent with the fact that LANDSAT 7 ACCA method is an enhancement compared to

251 LANDSAT 5. Four case studies are shown on Figures 7 ,8, 9, and 10. Figures 7, 8 and 9, correspond

252 to images for which the MTCD cloud cover is much greater than the ACCA one. On figures 7 and 8

253 the MTCD cloud mask seems quite accurate and the ACCA value is obviously underestimated. On

254 figure 9, the result assessment is more subjective. The left part of the image is very likely covered

255 by thin clouds, but the surface beneath is still visible. In such a case, our choice is to flag these

256 pixels as cloudy: thanks to VENμS and SENTINEL-2 frequent repetitivity, it is likely that another

257 cloud free image will be available just before or after this one.

258 In a very limited number of cases (one for each site), the ACCA provides a greater cloud cover than

259 MTCD. These cases happen when some snow cover is present like in figure 10 right. Even if the

260 cloud masks agree for simple cases like figure 10 left, some disagreements are observed in some

261 complex cases such as figure 10 right where thin clouds are above snow. The MTCD cloud and

262 snow detection seems accurate whereas the origin of the overestimation of the ACCA cloud mask is

263 difficult to tell, as only the cloud percentage obtained by ACCA is available.

264 5. Summary and Conclusions

265 A Multi-Temporal Cloud Detection method (MTCD) has been developed in the framework of the

266 preparation of VENμS and SENTINEL-2 Level 2 processors. The MTCD method makes a full use

267 of VENμS and SENTINEL-2 capacity for producing time series of images, with a frequent revisit

268 and under constant viewing angles. The algorithm is mainly based on a threshold on reflectance

269 temporal variation in the blue band, but is complemented by a few criteria designed to avoid false

270 detections : comparison of reflectance variations in the blue and in the red spectral bands, and a test

271 of the local correlation between the image to classify and the previously acquired images.

272 The method has been tested on two types of satellites, FORMOSAT-2 and LANDSAT 5 & 7, using

273 the same parameter set. The validation of this cloud mask was made by visual inspection and by

274 comparison with the cloud notation performed for the FORMOSAT2 and LANDSAT data catalogs.

275 For FORMOSAT-2, the results obtained with MTCD compare well with the visual notation

276 performed manually by operators at NSPO. For most of the disagreeing cases, a visual inspection

277 shows that MTCD is more accurate. Compared to the Automatic Cloud Cover Assessment (ACCA)

278 from LANDSAT data catalog, the cloud cover assessed by MTCD is almost always greater than that

279 of ACCA method. In most of the studied cases, the MTCD is more accurate : this is a good

280 performance, all the more so as the ACCA algorithm uses LANDSAT thermal infrared band, while

281 we did not allow ourselves to use it because neither VENμS or SENTINEL-2 offer such a band.

282 Some part of the differences between MTCD and ACCA masks are also related to our choice to

283 provide the user with a very stringent cloud mask : the MTCD cloud mask is designed to be

284 distributed with the product, and is also a preliminary step to perform accurate atmospheric

285 corrections. This algorithm has been tuned to flag even very thin clouds, but even though, the

286 amount of false detections remains low thanks to the good discrimination provided by the multi-

287 temporal variation criteria.

288 However, the good discrimination capability of the MTCD algorithm has a drawback: for an

289 operational ground segment, the MTCD method requires to process data in chronological order

290 which limits the possibilities to process the images in parallel. Still, the MTCD method will be

291 operationally used in VENμS ground segment for the production of level 2 products. Such a

292 decision has not yet been taken for SENTINEL-2.

293 For the time being, we applied the MTCD method to the high resolution satellites that can produce

294 time series with constant viewing angles (LANDSAT and FORMOSAT-2), but the availability of

295 VENμS and SENTINEL-2 will give more opportunities for improvements : VENμS will offer a

296 stereoscopic cloud mask thanks to two identical spectral bands with a viewing angle difference of

297 about 1.5 degree, whereas SENTINEL-2 will bring a spectral band at 1.38 μm which will enhance

298 detection of high clouds.

299 6. Acknowledgments

7. References

- S.A. Ackerman, K.I. Strabala, W.P. Menzel, R.A. Frey, C.C. Moeller, and L.E. Gumley (1998), "Discriminating clear sky from clouds with MODIS," Journal of Geophysical Research, vol. 103, pp. 32,141-32,157.
- S. Baillarin, P. Gigord, et O. Hagolle (2008), "Automatic Registration of Optical Images, a Stake for Future Missions: Application to Ortho-Rectification, Time Series and Mosaic Products," *IEEE International Geoscience and Remote Sensing Symposium, 2008.* vol. 2 1112-1115
- F.M. Bréon et S. Colzy (1999), "Cloud detection from the spaceborne POLDER instrument and validation against surface synoptic observations," Journal of Applied Meteorology, vol. 38, 777-785.
- F. Cabot, O. Hagolle, H. Cosnefroy, et X. Briottet (1998), "Inter-calibration using desertic sites as a reference target," *IEEE International Geoscience and Remote Sensing Symposium Proceedings, 1998.* vol.5., 2713-2715
- G. Dedieu, A. Karnieli, O. Hagolle, H. Jeanjean, F. Cabot, P. Ferrier, et Y. Yaniv (2006), "Venµs : A joint Israel-French Earth Observation scientific mission with High spatial and temporal resolution capabilities," Recent Advances in Quantitative Remote Sensing, Valencia, Spain: J.A.Sobrino, 517-521.
- J. Dozier (1989), "Spectral signature of alpine snow cover from the Landsat Thematic Mapper," *Remote Sensing of Environment*, vol. 28, 1989, 9–22.
- B.C. Gao (1993), A.F.H. Goetz, et W.J. Wiscombe, "Cirrus cloud detection from airborne imaging spectrometer data using the 1.38 µm water vapor band," Geophysical Research Letters, vol. 20, 1993, 301-304.
- J.I. Fisher, J.F. Mustard, and M.A. Vadeboncoeur (2006), "Green leaf phenology at Landsat resolution: scaling from the field to the satellite," Remote Sensing of Environment, vol. 100, 2006, pp. 265-279.
- R. Irish (2000), "Landsat 7 automatic cloud cover assessment," SPIE proceedings series, SPIE, vol. 4049, 348-355
- R.R. Irish, J.L. Barker, S.N. Goward, et T.J. Arvidson (2006), "Characterization of the Landsat-7 ETM Automated Cloud-Cover Assessment (ACCA) Algorithm," *Photogrammetric Engineering & Remote Sensing*, vol. 72 ,1179-1188
- O. Hagolle, G. Dedieu, B. Mougenot, V. Debaecker, B. Duchemin, et A. Meygret (2008), "Correction of aerosol effects on multi-temporal images acquired with constant viewing angles: Application to Formosat-2 images," *Remote Sensing of Environment*, vol. 112, 1689-1701.
- B. Hollingsworth, L. Chen, S.E. Reichenbach, et R. Irish (1996), "Automated cloud cover assessment for Landsat TM images," Proceedings of SPIE, Vol. 2819, 170-179.
- L. Lavanant, P. Marguinaud, L. Harang, J. Lelay, S. Péré, et S. Philippe (2007), "Operational cloud masking for the OSI SAF global METOP/AVHRR SST product," *EUMETSAT meteorological satellite conference*, 24-28.
- C. Latry, C. Panem, et P. Dejean (2007), "Cloud detection with SVM technique," IEEE International Geoscience and Remote Sensing Symposium, 2007. 448-451.
- S. Le Hégarat-Mascle et C. André (2009), "Use of Markov Random Fields for automatic cloud/shadow detection on high resolution optical images," *ISPRS Journal of Photogrammetry and Remote Sensing*, vol. 64, 351-366.
- G. Lissens, P. Kempeneers, et F. Fierens (2000), "Development of a cloud, snow and cloud shadow mask for VEGETATION imagery," Proceedings of VEGETATION 2000 Symposium, pp. 3-6.
- A. Lyapustin, Y. Wang, et R. Frey (2008), "An automatic cloud mask algorithm based on time series of MODIS measurements," *Journal of Geophysical Research*, vol. 113, D16207.
- F. Maignan, F.M. Bréon, and R. Lacaze (2004), "Bidirectional reflectance of Earth targets: Evaluation of analytical models using a large set of spaceborne measurements with emphasis on the Hot Spot," Remote Sensing of Environment, vol. 90 pp. 210-220.
- P. Martimor, O. Arino, M. Berger, R. Biasutti, B. Carnicero, U. Del Bello, V. Fernandez, F. Gascon, P. Silvestrin, et F. Spoto (2007), "Sentinel-2 optical high resolution mission for GMES operational services," IEEE International Geoscience and Remote Sensing Symposium, 2677-2680.
- M. Reuter et J. Fischer (2004), "Identification of cloudy and clear sky areas in SEVIRI Images" *Geophysical Research Abstracts*, EGU 2004 Conference, Nice, 05270.

356   • R.W. Saunders et K.T. Kriebel (1988), "An improved method for detecting clear sky and cloudy radiances
357 from AVHRR data," *International Journal of Remote Sensing*, vol. 9, 123-150.
358   • B. Wang, A. Ono, K. Muramatsu, and N. Fujiwara (1999), "Automated detection and removal of clouds
359 and their shadows from Landsat TM images," IEEE TRANSACTIONS on Information and Systems, vol. 2,
360 pp. 453-460.
361   • E.H. Wilson and S.A. Sader (2002), "Detection of forest harvest type using multiple dates of Landsat TM
362 imagery," Remote Sensing of Environment, vol. 80, pp. 385-396.
363   • http://landsathandbook.gsfc.nasa.gov/handbook.html, Landsat 7 science data users handbook,
364 NASA.

8. Tables

Table 1 Summary of the characteristics of sensors used in this study

	VENμS	FORMOSAT-2	SENTINEL-2	LANDSAT 5+7
Multispectral Resolution	10 m	8 m	10-20-60 m	30 m
Repetitivity(days) with constant viewing angles	2	1	10 (1 satellite) 5 (2 satellites)	16 (1 satellite) 8 (2 satellites)
Field of view (km)	24	27	300	180
Spectral bands (approximate center, nm).	412, 443, 490, 560, 620, 667, 702, 742, 782, 865, 910	485, 566, 660, 819	443, 490, 560, 665, 705, 740, 775, 842, 865, 940, 1375, 1610, 2200	485, 565, 665, 820, 1650, 2190, 11400
Coverage	50 to 100 sites	a few sites	All lands	All lands
Launch date	2012	2004	2013 (Sentinel 2A), 2014 (Sentinel 2B)	1984 (Landsat 5) 1999 (Landsat 7)

Table 2 Coordinates of the sites used in this article. The latitude and longitude of scene centre are provided, and for LANDSAT, the coordinates in World Reference System 2 (WRS-2) are provided.

Site, Country	Satellite	Latitude-longitude	Path-Row coordinates (LANDSAT)
Muret, France	FORMOSAT	43.48, 1.18	
Tensift, Morocco	FORMOSAT	31.67,-7.60	
Boulder, USA	LANDSAT	40.25, -104.25	033 - 032
Columbia, USA	LANDSAT	34.45,-82.5	017 - 036
Fresno, USA	LANDSAT	36.15,-119.5	042 – 035
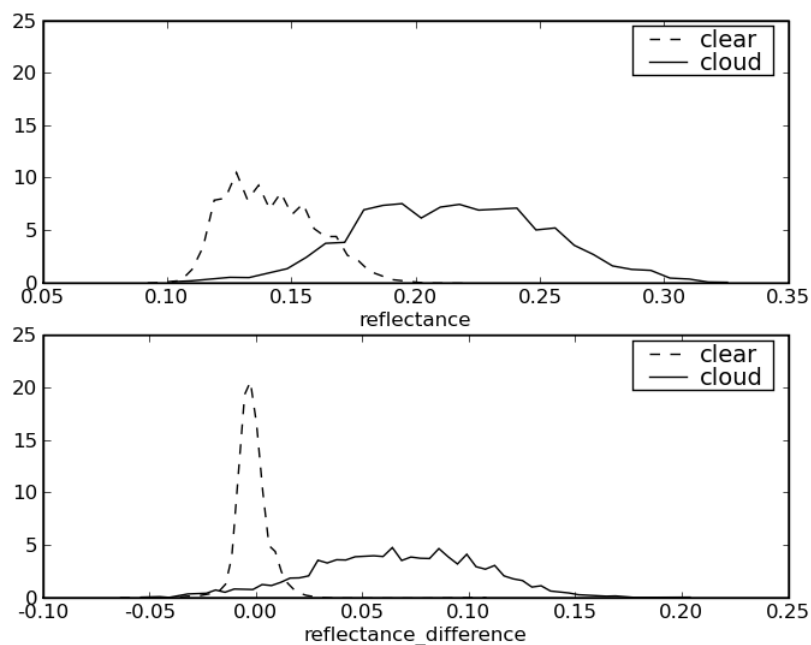
9.Figures

Figure 1 :Comparison of histograms of clouded and unclouded pixels for FORMOSAT-2 blue band on Tensift site (Morocco), top : absolute reflectance on the April 13th, 2006, bottom: reflectance variation between the April 1st and the April 13th 2006. The image on April 1st is completely cloud free. Pixels within cloud shadows are not taken into account in the histograms.
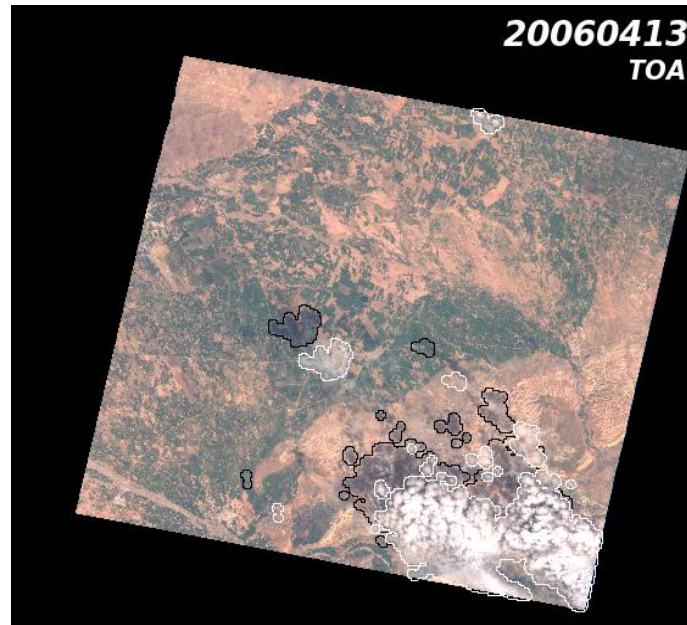
Figure 2: color composite of FORMOSAT-2 red, green and blue Top of Atmosphere (TOA) reflectances for Tensift scene acquired on April 13th, 2006. Clouds detected by Multi Temporal Cloud Detection (MTCD) method are circled in white and cloud shadows are circled in black.
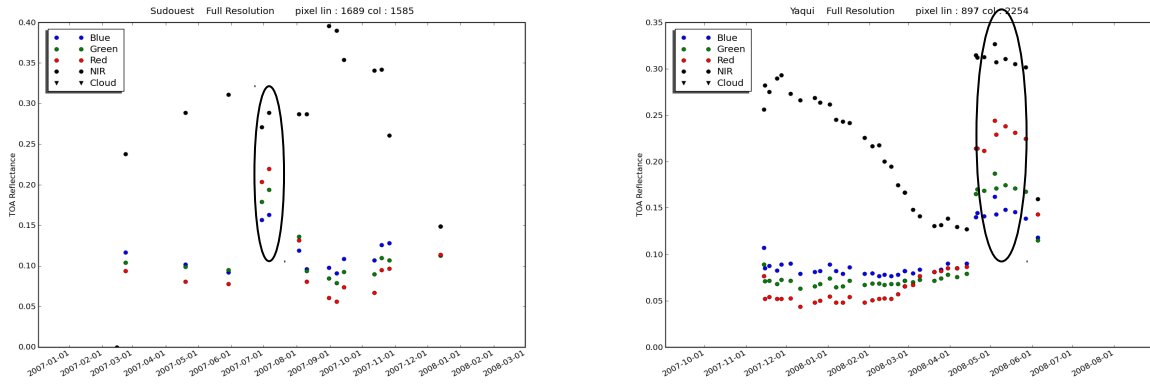
Figure 3: Temporal profile of cloud free TOA reflectances from FORMOSAT-2, left) for a pixel in a sorghum field near Muret (France), Right) for a wheat Field near Yaqui Mexico. On the left plot, the field is ploughed at the end of June, and before that date, was covered with sparse vegetation, on the right plot, the pixel is a wheat field which is cropped in may. For both sites and both dates, the test on the red variation corresponding to equation (2) prevents the circled pixels to be flagged as a cloud by the test on the Blue reflectance variation (equation 1).
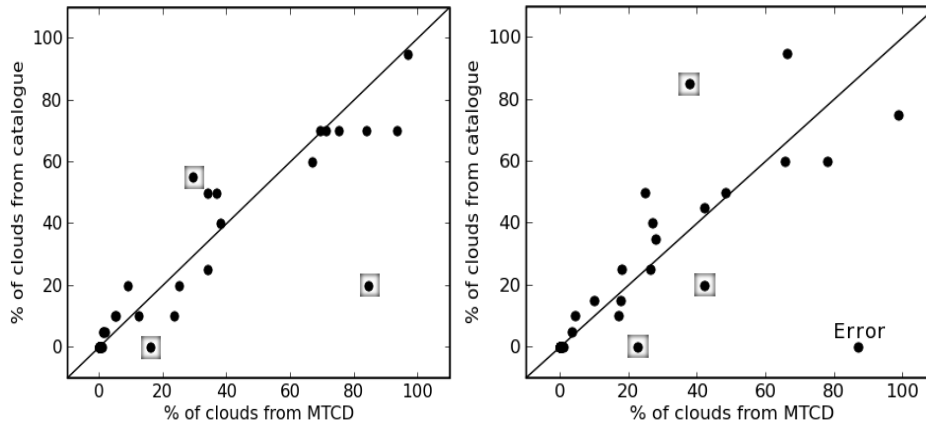
Figure 4 : comparison of the percentage of cloudy pixels on FORMOSAT-2 images estimated during NSPO manual cloud notation with the cloud percentage estimated by our multi-temporal method. Left, for Muret time series in France, Right for Tensift Time series. Large squares correspond to case studies shown on Figure 5, while the dot marked "error" corresponds to an obvious notation error from NSPO.
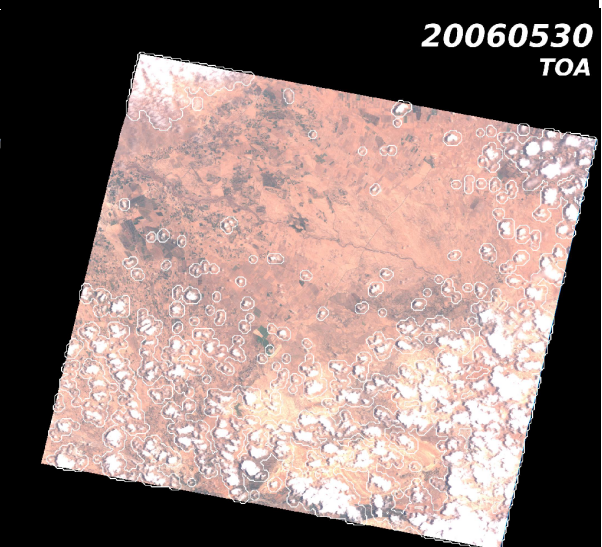
372
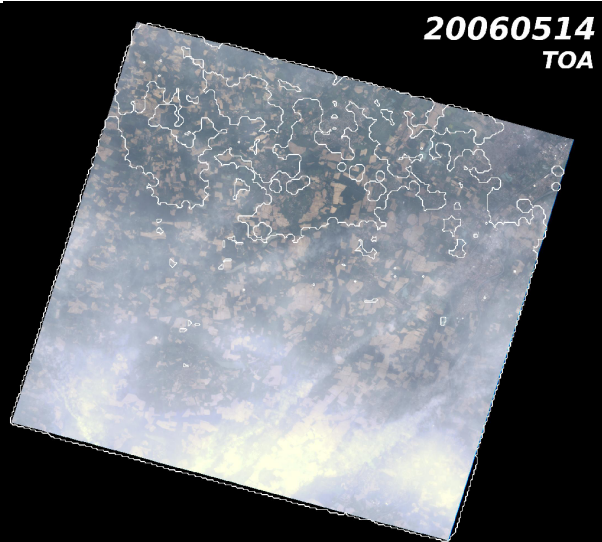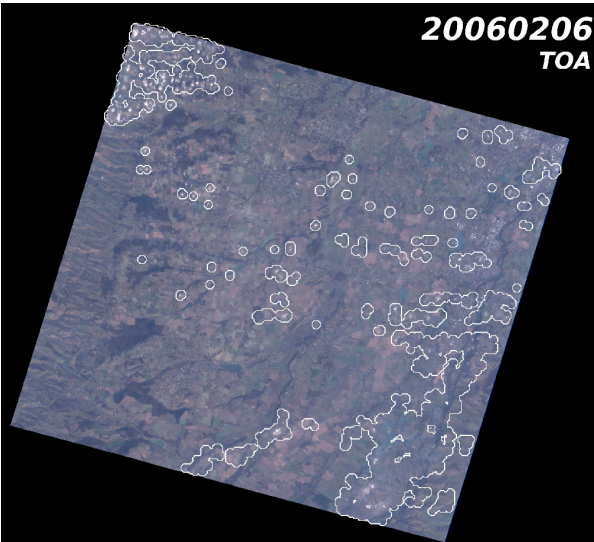
373
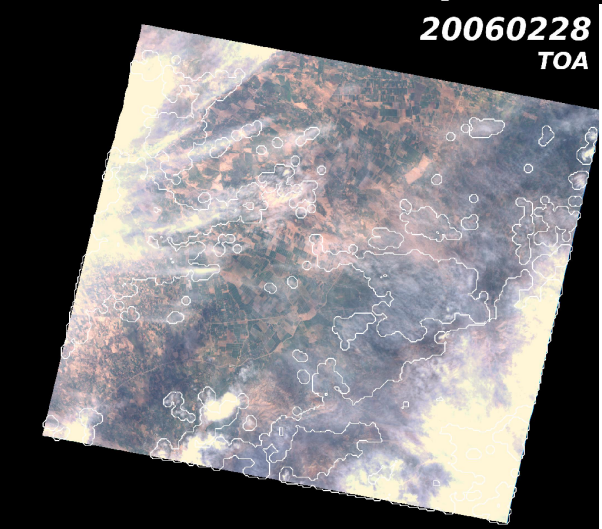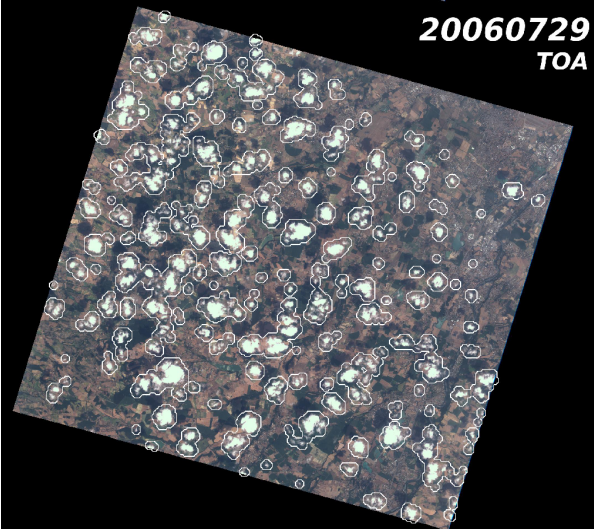
374

Figure 5 : visual verifications for a few cases identified in figure 3. White lines correspond to cloud contours from MTCD method. Upper Left) MTCD gives 12% of cloud cover, NSPO: 0%. Very small clouds can be seen, that were not seen by the operator. Upper Right) MTCD 80%, NSPO: 20%. Here, the operator probably only considered the thick clouds at the bottom of the image, but most of the image is evidently covered by thin clouds. Middle left) MTCD : 34%, NSPO 55%. The image is covered by small clouds, all of them seem to have been detected by MTCD. The operator has probably considered part of the space between clouds as cloudy. Middle right) MTCD 37%, NSPO 85%, the thin cloud cover is underestimated by our cloud mask because the previous image in the time series is quite old. Bottom Left) MTCD 22%, NSPO 0% . Thin clouds were not classified as clouds by NSPO operator. Bottom Right) MTCD 42%, NSPO 20%. The MTCD cloud cover looks accurate.

375
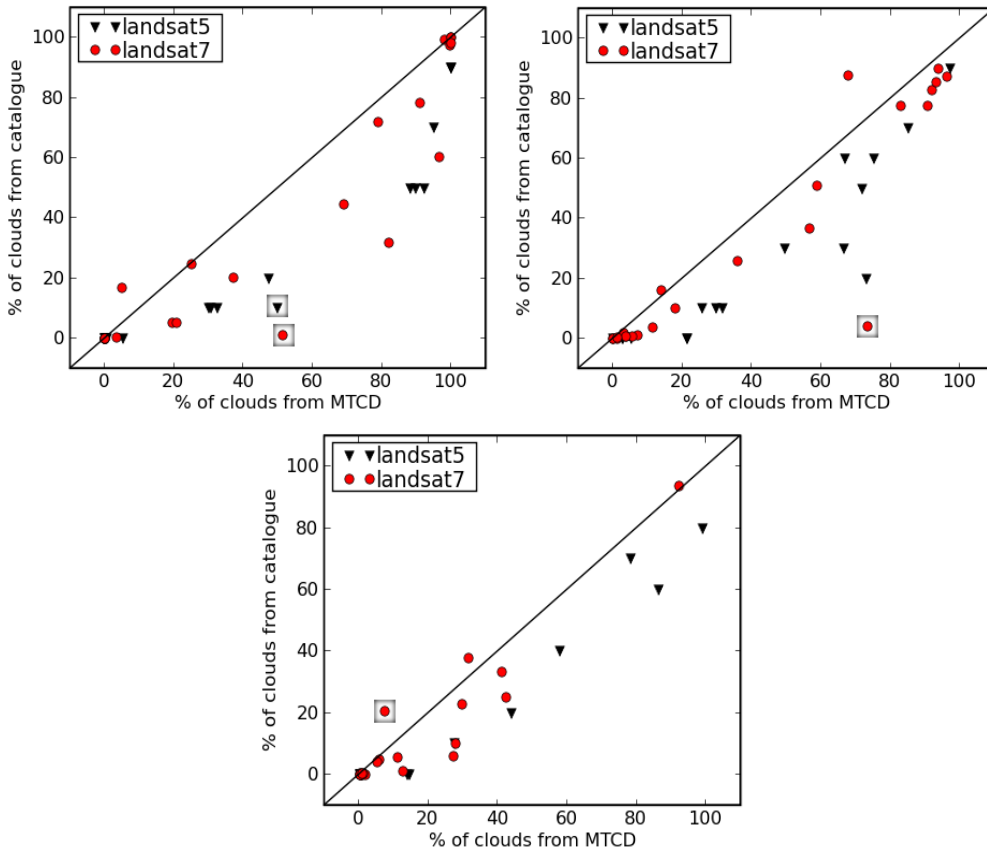
376

Figure 6 : Comparison of MTCD cloud cover percentage to LANDSAT ACCA algorithm from the LANDSAT catalog, left, on Columbia site (USA), right on Boulder site (USA), Bottom on Fresno site (USA) for all the images acquired in 2002. Circles correspond to LANDSAT 7, whereas triangles correspond to LANDSAT 5. Note that many points are in agreement when cloud percentage is close to 0 or 100. The large squares correspond to the images analyzed below (Figures 7 ,8, 9, and 10)
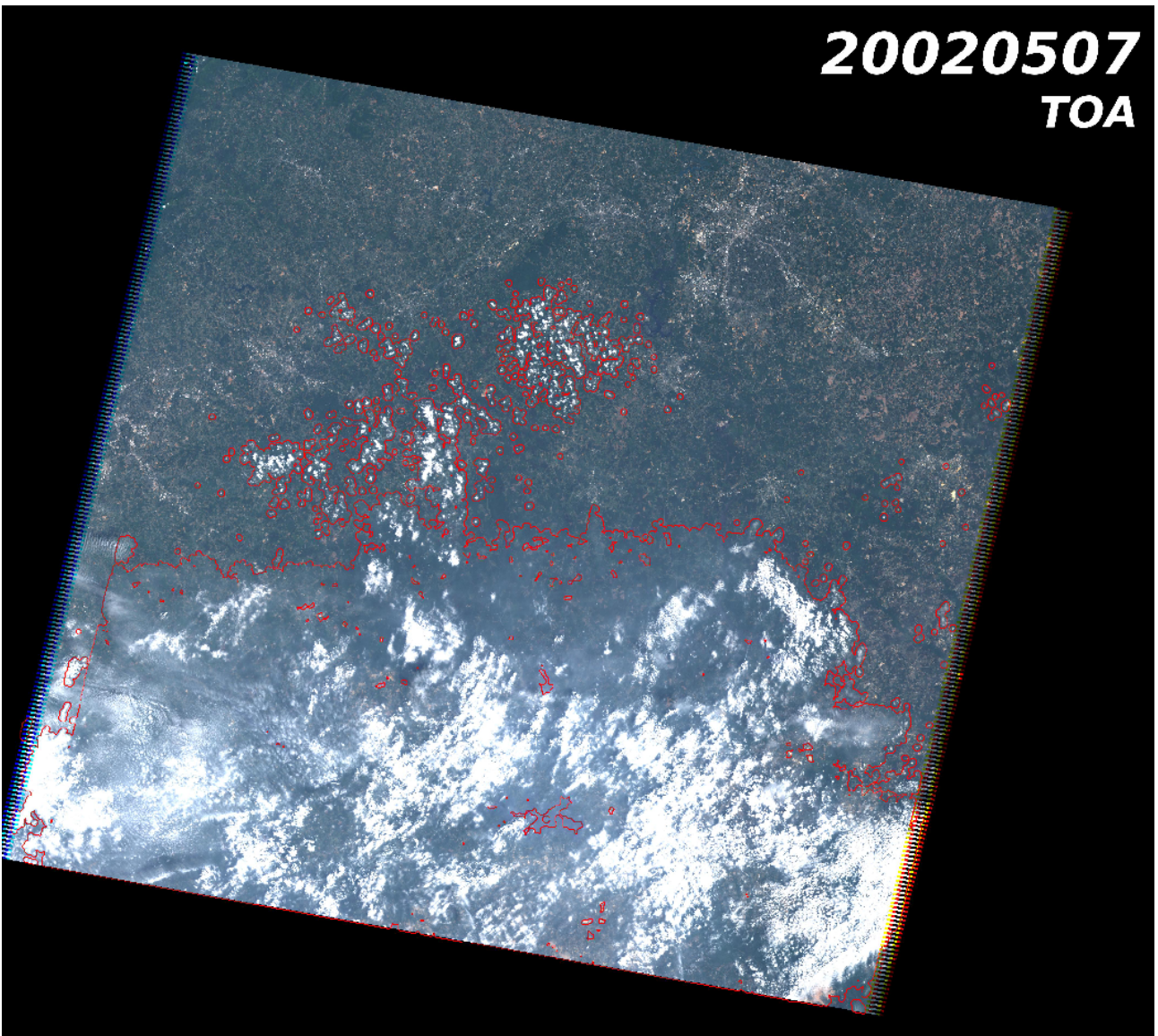
377

Figure 7 :LANDSAT 5 image near Columbia, South Carolina, USA, for which cloud cover is 10% according to ACCA method and 49% according to MTCD method. Red lines correspond to MTCD image contours. The ACCA percentage is clearly underestimated.
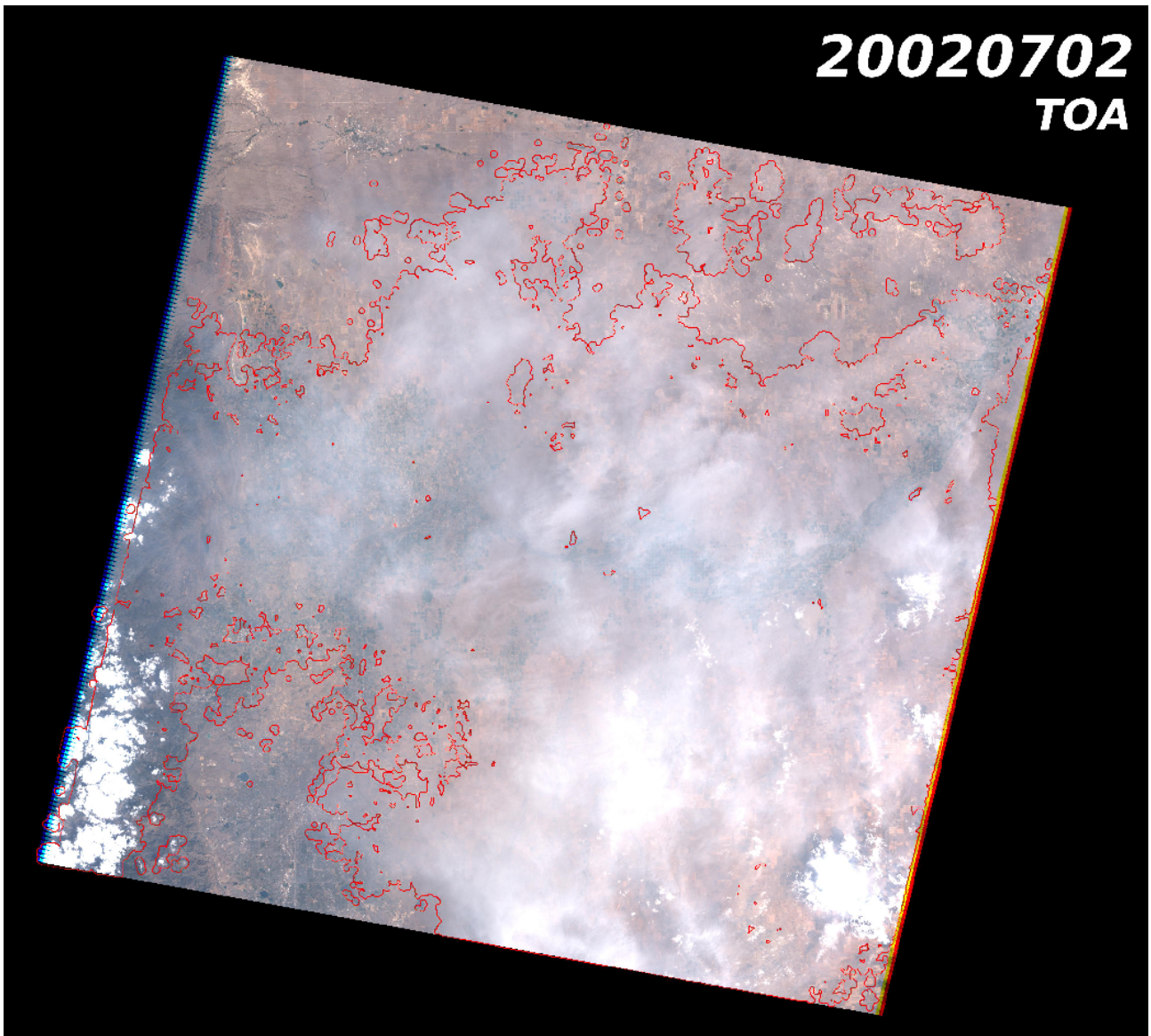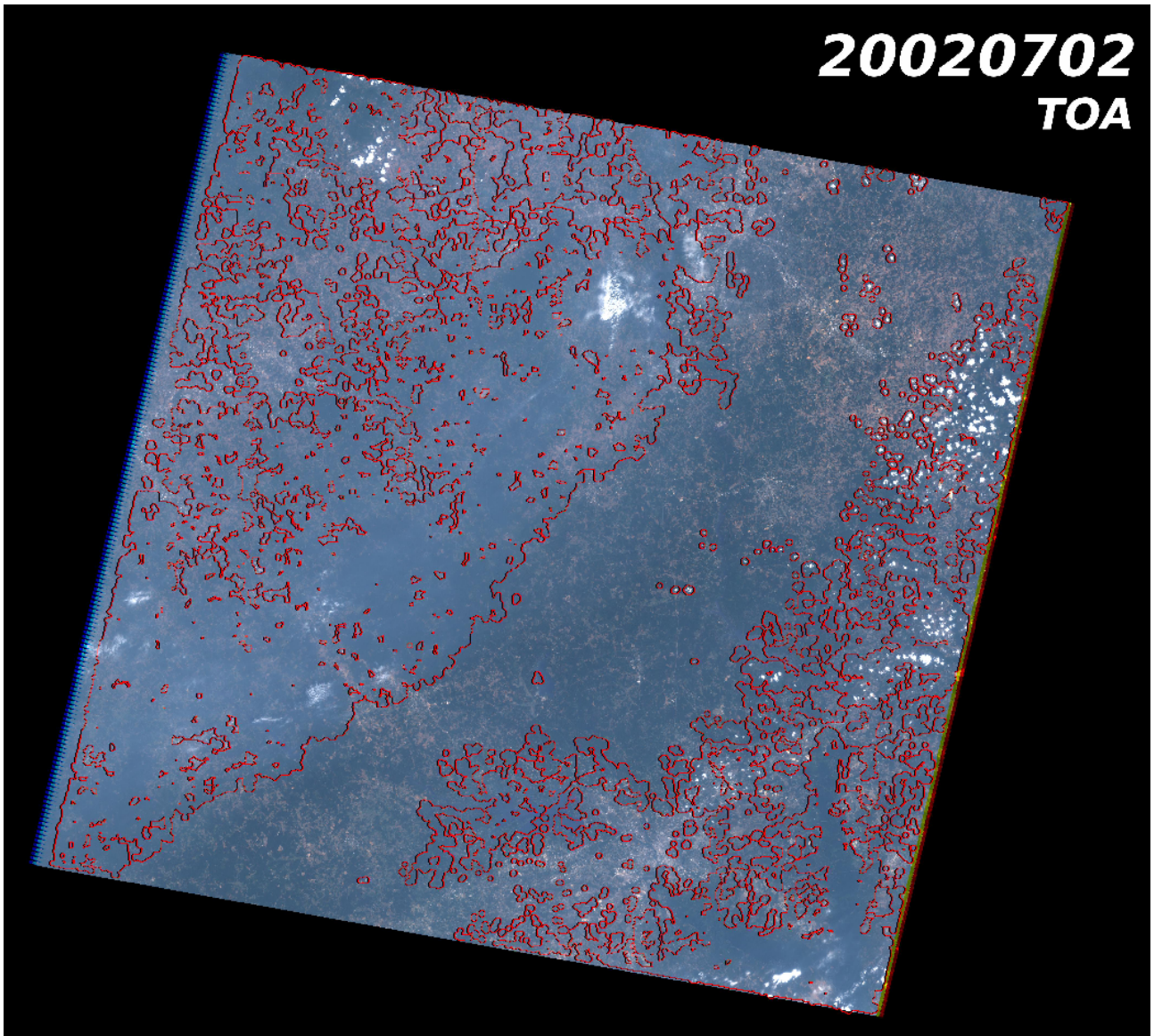
Figure 8 :LANDSAT 7 image near Boulder USA, for which cloud cover is 4% according to data catalogue and 73% according to MTCD method. Red lines correspond to MTCD image contours. The ACCA percentage is clearly underestimated, and even the MTCD cloud mask misses some semi-transparent clouds in the upper left corner of the image.

378

Figure 9 :LANDSAT 7 image near Columbia, South Carolina, USA, for which cloud cover is 1.7% according to data catalogue and 51% according to MTCD method. Red lines correspond to MTCD image contours. Although the result of MTCD method is maybe too strict, and its appreciation might be subjective, the ACCA percentage is clearly underestimated.

379
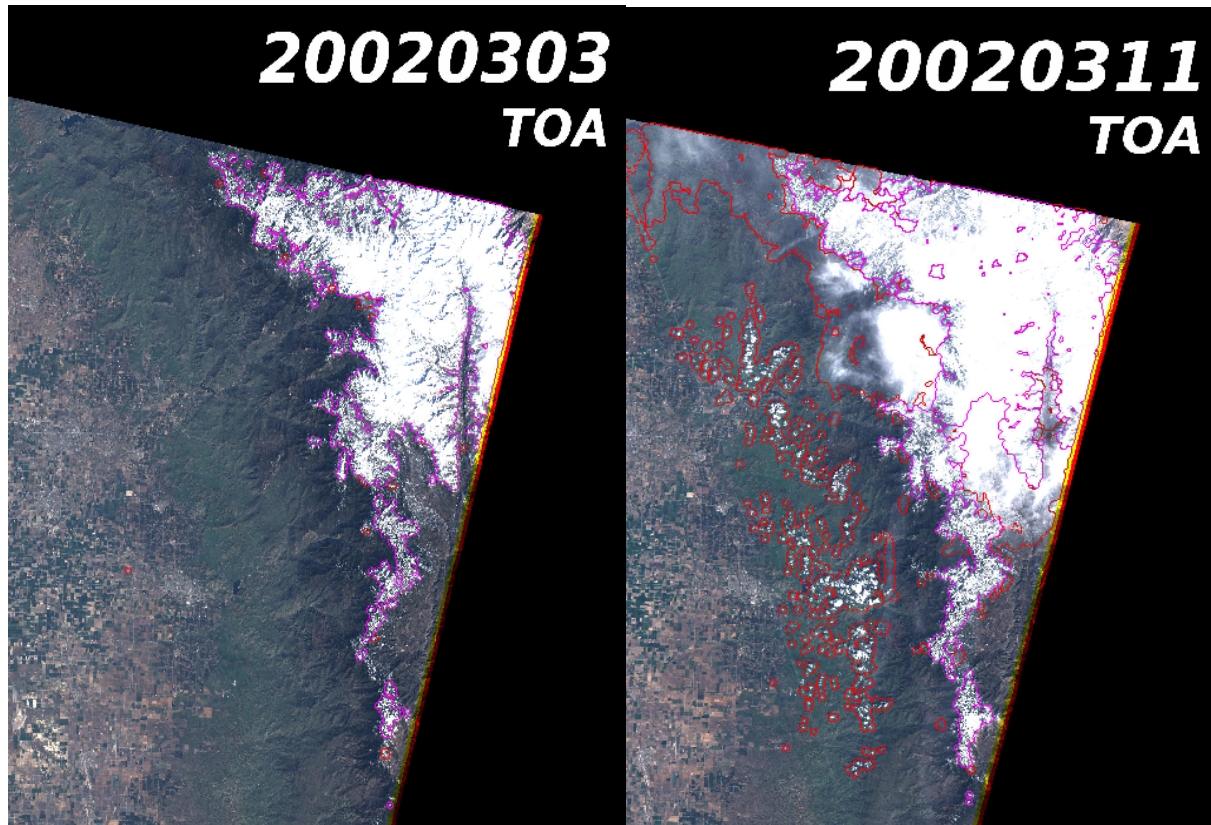
Figure 10 :LANDSAT 7 images extracts near Fresno California USA. Red lines correspond to MTCD image contours and pink lines to snow contours. On the image of the 3rd of March , ACCA and MTCD agree finding no cloud. For the image of the 11th of March, cloud cover is 20 % according to ACCA and 7% according to MTCD.   The MTCD cloud and snow mask seems accurate, although it is a complex case with clouds above snow. MTCD probably finds more snow than ACCA.

380